An elementary eye with optic flow detection and compositional properties

Ramon Pericet-Camara[1], Michal K. Dobrzynski[1], Raphaël Juston[2], Stéphane Viollet[2], Robert Leitel[3], Hanspeter A. Mallot[4], Dario Floreano[1,*]

[1]*Laboratory of Intelligent Systems, École Polytechnique Fédérale de Lausanne, Switzerland*

[2] *Aix-Marseille Université, CNRS, ISM UMR7287, 13288, Marseille CEDEX 09, France.*

[3]*Fraunhofer Institute for Applied Optics and Precision Engineering, Jena, Germany*

[4]*Laboratory of Cognitive Systems, Department of Biology, University of Tübingen, Germany*

*To whom correspondence should be addressed. E-mail: dario.floreano@epfl.ch

Abstract

We describe a 2-milligram artificial elementary eye whose structure and functionality is inspired by compound eye ommatidia. Its optical sensitivity and electronic architecture are sufficient to generate the required signals for the measurement of local optic flow vectors in multiple directions. Multiple elementary eyes can be assembled to create a compound vision system of desired shape and curvature spanning large fields of view. The system configurability is validated with the fabrication of a flexible linear array of artificial elementary eyes capable of extracting optic flow over multiple visual directions.

Keywords

Artificial vision; insect vision; compound eye; motion detection; optic flow; microengineering

Introduction

Insects have evolved vision systems with a large variety of morphologies and distribution on the animal head tailored to assist specific behaviours in their ecological niche[1]. The advantage of this variable spatial design with respect to vertebrate eyes is that it can offer such customized sensing over large fields of view combined with relatively small packages and fast extraction of motion information. Insect vision organs can be categorized in two main types: insect simple eyes or ocelli are individual organs made of a corneal refracting interface, often underlying a lens, which focuses light onto a variable number of photoreceptors, ranging from a handful in the *stemmata* of the annelid worms *polychaetes* to tens of thousands in some flying insect ocelli[1]. Ocelli can detect change in patterns of light intensity[2-4] and help in tasks like attitude stabilization [5]. On the other hand, compound eyes consist of an arrangement of tiny optical units called ommatidia, each composed of a microscopic

lens that focuses light on a small set of photoreceptors. Compound eyes are specialized in optic flow extraction from wide fields of view to assist in tasks like collision-free navigation, flight stabilization, and prey, predator or mate detection[1].

Vision systems that can be configured like insect eyes to suit specific tasks could provide useful information in an efficient manner for many applications where energy and payload constraints are drastic, such as micro flying robot navigation[6-8]. Curved artificial compound eyes made of hundreds of ommatidia have been recently described[9, 10] and tested for basic navigation control[8, 9]. These prototypes possess a fixed design since optic flow extraction over adjacent ommatidia puts strong constraints on the interommatidial angle and thus geometry of the compound eye. An arrangement of four phototransistors inspired by the three dorsal ocelli found in most flying insects was recently used to stabilize the attitude of a microflyer[11]. The four photodetectors used to compute the angular velocities of the robot encompassed a volume of 4x4x3.3 mm and yielded a non-customizable design. In another work, a Centeye's Tam4 optic flow sensor was used to control the altitude of a tethered microflyer, although this sensor extracts motion in only a single direction and has a size of approximately 3x3 mm^2 [12].

Here, we describe the design, fabrication, configurability, and use of an artificial elementary eye, partly inspired by the insect ommatidium, that can be combined in arrays with different geometries. In contrast to a single insect ommatidium, the artificial elementary eye can extract optic flow vectors in multiple directions by means of several suitably arranged photodetectors. This feature, which is loosely equivalent to a small cluster of neighbouring ommatidia or to a single ocellus, makes the elementary eye usable either as a standalone sensor or as an element of an artificial compound eye without constraints on the visual angle between adjacent elementary eyes. The sensor yields three photoreceptors under a single lens and bears a size of 1925x475x860µm and a weight of 2mg, which includes the optics and the photosensitive area with a total footprint diameter of 175 µm, an analog signal processing circuit for illuminance adaptation, an analog-to-digital signal conversion circuit, and a communication interface. The signal acquisition frequency of the elementary eye is 300 Hz, which allows for fast motion extraction. The photodetector sensitivity, analog processing circuitry, ADC components and communication interface of the sensor are similar to the ones of the artificial ommatidia columns in the sensor presented in Floreano *et al*[9].

Structure of the elementary eye

The artificial elementary eye was designed finding inspiration in the ommatidia of insect apposition compound eyes as natural local motion sensors. Each natural ommatidium consists of a lens, an elongated waveguide space known as rhabdom, and a small set of photoreceptors along the rhabdom. In the elementary eye (Figure 1 and S1), the focusing element consists of a moulded polymer microlens (Ormocomp, Micro Resist Technology GmbH, Berlin, Germany) placed on a 560 µm thick glass stack (display glass AF32, Schott AG), which guides light to the photosensitive areas of an optoelectronic silicon chip (Figure 1b). A characteristic of the elementary eye is that the optics have been designed such that the projected light on the photodetectors bears the same area as the photodetector footprint in order to optimize its sensitivity.

Models of motion detection [13, 14] in the retina of mammals[15] as well as in the compound eyes of arthropods[16] suggest that isolated pairs of photoreceptors provide information about motion along a single direction. Recently, it has been observed that the fly visual system extracts directional motion in the four cardinal directions using eight different local motion detectors, being the major or unique signal inputs to downstream neuropiles and motion-driven behaviours[16]. Inspired by these findings, we have endowed our elementary eye with a triplet of hexagonal photodetectors arranged so that their centres form the vertices of an equilateral triangle (Figure 1e and Figure S1). The unidirectional motion values issued by the three photodetector pairs can be combined to compute an optic flow vector in any direction of the image plane from the vision field of the elementary eye. A higher number of photodetectors could increase the precision of the optic flow extraction, but it would come at the cost of significantly increasing the elementary eye footprint. A lower number would not provide motion information in more than a single direction.

Diurnal flying insects perceive highly contrasted images of the surrounding world as a result of the 1:1 ratio between the interommatidial and the acceptance angle of their compound eyes. This characteristic provides them with an efficient motion extraction at fast speeds[17]. Our elementary eye was designed to yield acceptance and inter-detector angles inspired by the optical properties of the ommatidia in *Drosophila melanogaster*, where each ommatidium has an acceptance angle of 4.5 degrees[18] and an interommatidial angle of 4.7-5.5 degrees[19] (see Supp Info for further details on Microoptics design).

Natural ommatidia bear pigmented sidewalls that prevent light rays other than those refracted by the lens from arriving at the photodetectors. In the elementary eye, this function is played by a diaphragm layer inside the glass stack (Figure 1b) and an opaque glob-top encapsulation polymer on the sidewalls (Figure 1d) blocking light that does not come directly from the upper optical aperture.

In a natural visual scene, illumination may have a dynamic range up to eight decades. To avoid saturation due to illumination changes, each photodetector is connected to an adaptive analogue VLSI circuit featuring a large dynamic range at ultra-low-power processing[20] (Figure S1a,b). A first-order, low-pass filter prevents temporal aliasing and keeps the photodetector bandwidth at 300 Hz. The electronic die also includes a bias circuit, a 10-bit analogue-to-digital converter (ADC), and a logic circuit implementing a serial interface for signal read-out. The self-contained elementary eye has a total surface of 0.9 mm^2, is 860 µm high, consumes 444 µA, and weighs less than 2 mg.

The optical and electronic components of the elementary eye are separately fabricated in large planar arrays, precisely aligned on top of each other so that each microlens focuses light only onto its corresponding photodetector triplet, individually cut and attached to a printed circuit board (PCB), following the same manufacturing procedure used in a previously described artificial compound eye[9, 21]. Every eye in the array has individual bond pads wired to the PCB for independent analog and digital voltage feed, as well as synchronization, clock, and data lines for serial read-out (Figure S1a). The PCB, wires, and encapsulation material add 54 mg to each artificial elementary eye, and could be further reduced to fit the requirements of specific applications.

Sensitivity to light incidence angle and intensity

To characterize the optics of the artificial elementary eye, we measured the angular sensitivity function (ASF) of each of the three photodetectors of a single prototype (Figure 2a; see also Characterization methods in Supplementary Information), which yield Gaussian profiles. We then measured the acceptance angles and inter-detector angles from the measured ASFs. The acceptance angle $\Delta\rho$ is defined by the full width at half maximum of the ASF. The inter-detector angle $\Delta\varphi$ is defined by the angular position of the peak of two adjacent ASFs (Figure 2a). The mean acceptance angle $\Delta\rho$ was 4.78° ± 0.22° and the mean inter-detector angle $\Delta\varphi$ was 5.52° ± 0.02°. The obtained 1.15:1 ratio lies in the range found in most diurnal flying insects, providing the elementary eye with adequate optical characteristics for optic flow extraction[17].

Figure 2b shows the mean steady state and transient responses of the elementary eye photodetectors to illuminance step increments and decrements presented at six different steady levels and covering nearly 6 decades of light irradiance. At five of these six levels (red circles in Figure 2b), the output response of the individual photodetector to light steps yields an S-shaped operating curve in a semi-log plot. The five S-shaped curves yield a similar slope, which demonstrates an analogous dynamic sensitivity at the five decades to sudden changes of illumination of about 1100 mV per decade in the linear part. Similar S-shape curves shifting for different background illuminations were also observed in biological photoreceptors[22, 23], preventing saturation by bright spots in the visual scene and enabling adaptation to sudden changes of illumination. The curve at the lowest irradiance (10^{-8} W/cm^2) was obtained by means of an additional neutral density filter with an attenuating factor of 10^{-4} (see Characterization methods in Supplementary Information) yielding a response at only 0.1lux. The different shape of this last curve is probably due to the influence of the photodetector dark current at this luminosity level.

Optic Flow Extraction

The artificial elementary eye has been designed following optical parameters of fruit fly ommatidia that enable it to extract the optic flow. We characterize this capability by making it rotate in the middle of an arena surrounded by a circular wall covered with random pattern images (Figure 3a). Theoretically, the optic flow under such pure rotational motion must be directly proportional to the rotational speed[24]. In the experimental setup, the elementary eye is embedded in a robotic device with the photodetector triplet plane perpendicular to the ground and parallel to the arena walls (Figure 3a). The sensor can be fixed at four different angles α around its roll axis with respect to the arena walls (Figure 3a and Figure 4a) so that the optic flow extraction in four different directions at the triplet plane can be assessed. In the experiment, the robot performs yaw rotations for every eye angle position α at several constant speeds ω while the visual signals are registered in a memory card. Frames containing the three values of the triplet signals were recorded at a rate of 350 frames per second (fps) during the experiments. The optic flow is calculated out of the recorded frames offline in an external computer using Matlab (Mathworks, MA, USA).

In this work, an ad-hoc method is utilized to calculate the optic flow. For this, the artificial elementary eye is broken down in three unidirectional motion sensors formed by the three pairs of photodetectors, which bear a fixed inter-detector angle $\Delta\varphi$ between their viewing directions (see Figure 2a). It is considered that a photodetector unit *i* of the pair will sample scene sections during motion with a time difference Δt_{ij} with respect to the contiguous paired photodetector *j* (Figure 3b). At an inter-detector angle $\Delta\varphi$, the signal time delay Δt_{ij} at every pair is inversely proportional to the optic flow $\overline{OF}$ projected onto the vector $\overline{r_{ij}}$, which connects the photodetector pair (Figure 3b, inset):

$$\Delta t_{ij} = \frac{\Delta\varphi}{\overline{OF} \cdot \overline{r_{ij}}}$$

The OF_x and OF_y optic flow vector components, which are the searched final outcome, can be expressed using the X and Y components of the pair connector r_{ij}^x and r_{ij}^y as:

$$\Delta t_{ij} = \frac{\Delta\varphi}{OF_x \cdot r_{ij}^x + OF_y \cdot r_{ij}^y}$$

If we apply this expression to the three pairs of photodetectors, we obtain a system of three equations and two unknowns, OF_x and OF_y:

$$\begin{cases} \left(OF_x \cdot r_{12}^x + OF_y \cdot r_{12}^y\right) \cdot \Delta t_{12} = \Delta\varphi \\ \left(OF_x \cdot r_{23}^x + OF_y \cdot r_{23}^y\right) \cdot \Delta t_{23} = \Delta\varphi \\ \left(OF_x \cdot r_{31}^x + OF_y \cdot r_{31}^y\right) \cdot \Delta t_{31} = \Delta\varphi \end{cases}$$

which can be reduced to the expression

$$A \cdot \vec{OF} = \vec{b}$$

where

$$A = \begin{bmatrix} \Delta t_{12} \cdot r_{12}^x & \Delta t_{12} \cdot r_{12}^y \\ \Delta t_{23} \cdot r_{23}^x & \Delta t_{23} \cdot r_{23}^y \\ \Delta t_{31} \cdot r_{31}^x & \Delta t_{31} \cdot r_{31}^y \end{bmatrix}, \qquad \vec{b} = \begin{bmatrix} \varphi \\ \varphi \\ \varphi \end{bmatrix}$$

From these, the optic flow vector can be calculated using the least squares method:

$$\overrightarrow{OF} = [A^T A]^{-1} \cdot A^T \cdot \vec{b}$$

Δt_{ij} can be obtain from the frame difference Δf_{ij} (see Figure 3b) using the sensor frame rate in the expression:

$$\Delta t_{ij} = \frac{\Delta f_{ij}}{350\ fps}$$

In the experimental visual data, we search Δf_{ij} that minimizes the mean squared error between the photodetector signals of the ij pair in data windows of 350 points, that is, one experimental second, for the whole 30 seconds of the experiment. The optic flow values identified in the 30-second period are collected and the mean and standard deviations for the optic flow vector module and for the angle are plotted against the constant rotational speed of the robot (Figure 4b,c).

As predicted by theory[24], the norm of the measured optic flow matches the yaw rotational speed, regardless of the roll angle at which the elementary eye is fixed (Figure 4b), and the optic flow angle matches well the roll angle in the four studied cases (Figure 4c). The increasing standard deviation of the OF angles at lower rotational speeds are likely due to the light adaptation mechanism of the analog VLSI circuit[20, 25], which yields an exponential decay of the signal over time in the absence of visual contrast. At low rotational speeds, there is higher probability of spending longer time pointing at featureless areas of the visual scene, thus yielding small errors in the extraction of optic flow angle.

The capability of the artificial elementary eye to extract vectors of optic flow is demonstrated in an environment displaying natural-like features and of about 400 lux of illuminance, which corresponds approximately to the illumination of a standard office. Nevertheless, the light sensitivity of the elementary eye is practically similar along five decades of irradiance thanks to the adaptability provided by the implemented Delbruck circuit (see Figure 2b). Thus, it can be certainly claimed that the sensor is fully functional to extract optic flow at those illumination conditions, too. However, further work is needed to test alternative conditions, e.g. an environment where features yield lower contrast. Furthermore, the utilized processing method requires a computational power that is inadequate to be used in small-size embedded real-time systems. Future work will investigate algorithms that can be implemented in small ASICs beside the elementary eye and compute motion for real-time tasks.

A flexible array of artificial elementary eyes

Many functionally independent artificial elementary eyes could be arranged in morphologically different configurations to span large fields of view. For example, here we show a linear configuration of eyes for motion extraction over large fields of view on the horizontal plane. The device consists of a flexible printed circuit board

with two linear arrays of 34 artificial eyes and a microcontroller (Microchip® dsPIC33FJ128GP802, Chandler, AZ, USA) to collect and process signals (Figure 5a). In this case, the fabrication procedure is identical to that described above, with the exception that cutting of the individual elementary eyes does not impact the flexible PCB, which includes the electric lines to carry the signals to the microcontroller. The flexible array can undergo reversible mechanical bending down to a radius of curvature of approximately 6 mm. Mechanical flexibility allows the sensor array to span a variable field of view, whose range is limited by the mechanical properties of the PCB.

The eye array was attached to the front side of a cylindrical wheeled robot, yielding a field of view of 135° along the horizontal direction and of 5.2° along the vertical direction (Figure 5b). Visual signals were acquired from a subset of 11 elementary eyes uniformly distributed along the sensor while the robot moved on a straight trajectory at 8 cm/s in the centre of a corridor with textured walls (Figure S2). Optic flow measured offline from the selected eyes sampled at 130 frames/s (Figure 5c) show that optic flow vectors from eyes closer to the extremities of the array display an angular orientation parallel to the ground and larger intensities, as predicted by optic flow patterns in translation[24].

Discussion

Despite its microscopic size and narrow field of view, the artificial elementary eye described here can extract local optic flow vectors at high speed, different lighting conditions, and at low power. Further miniaturization of the eye could be possible. For example, the sensor footprint could be reduced by re-arranging the electronics layout, which, in the prototype presented here, has been optimized for a linear layout of multiple eyes. Also, the area of the photodetectors could be reduced, which would result as well in a lower eye height in order to keep the match between the projected light area and that of the photodetector footprint, albeit at the cost of lower sensitivity in dark environments. Finally, high-end CMOS fabrication processes could result in further size reduction of the embedded microelectronic circuitry and components, and the relatively large wire bond pads could be replaced by through-silicon-vias or flip-chip bonding.

The visual capabilities of the artificial elementary eye could be used for autonomous flight of microrobots[6], provide visual odometry to medical endoscopes, estimate incoming collisions in wearable alert systems, and many other applications that require fast motion detection in a small and lightweight package[26]. Artificial elementary eyes could also be embedded on the surface of soft and flexible robots with minimal impact on their mechanical properties, or arranged in flexible layers that can be adapted to arbitrary shapes, as shown with the linear array presented here, or embedded in smart clothing. Finally, artificial elementary eyes could also be aggregated on curved rigid surfaces to form artificial compound eyes with variable spatial density as required by the environment and motion of the agent, mimicking the diversity and evolution of biological compound eyes.

Authors' contributions

RPC, SV, RL, HAM, and DF conceived, designed and supervised the project. RPC and RJ set up and performed experiments. MKD and RL built prototypes. RPC, SV,

HAM and DF analysed data. RPC and DF wrote the paper with assistance from SV, RL and HAM.

Acknowledgements

We acknowledge financial support of European project FET-Open grant number 237940 and of the Swiss National Centre of Competence in Research Robotics (NCCR). We thank Wolfgang Buß, Felix Kraze, and Julien Diperi for the realization of various assembly tasks, Marc Boyron, Grégoire Heitz, and Géraud L'Eplattenier for electronic design and fabrication, and Bryan Schubert for proofreading.

We have no competing interests.

References

[1] Land, M.F. & Nilsson, D.-E. 2002 *Animal eyes*. Oxford, Oxford University Press.

[2] Warrant, E.J., Kelber, A., Wallén, R. & Wcislo, W.T. 2006 Ocellar optics in nocturnal and diurnal bees and wasps. *Arthropod Struct Dev* **35**, 293-305. (doi:10.1016/j.asd.2006.08.012).

[3] Parsons, M.M., Krapp, H.G. & Laughlin, S.B. 2006 A motion-sensitive neurone responds to signals from the two visual systems of the blowfly, the compound eyes and ocelli. *J. Exp. Biol.* **209**, 4464-4474. (doi:10.1242/jeb.02560).

[4] Schuppe, H. & Hengstenberg, R. 1993 Optical properties of the ocelli of Calliphora erythrocephala and their role in the dorsal light response. *J Comp Physiol A* **173**, 143-149. (doi:10.1007/bf00192973).

[5] Berry, R.P., Stange, G. & Warrant, E.J. 2007 Form vision in the insect dorsal ocelli: An anatomical and optical analysis of the dragonfly median ocellus. *Vision Res.* **47**, 1394-1409. (doi:10.1016/j.visres.2007.01.019).

[6] Ma, K.Y., Chirarattananon, P., Fuller, S.B. & Wood, R.J. 2013 Controlled Flight of a Biologically Inspired, Insect-Scale Robot. *Science* **340**, 603-607. (doi:10.1126/science.1231806).

[7] Gremillion, G., Humbert, J.S. & Krapp, H. 2014 Bio-inspired modeling and implementation of the ocelli visual system of flying insects. *Biol Cybern*, 1-12. (doi:10.1007/s00422-014-0610-x).

[8] Expert, F. & Ruffier, F. 2015 Flying over uneven moving terrain based on optic-flow cues without any need for reference frames or accelerometers. *Bioinspiration Biomim* **10**, 026003.

[9] Floreano, D., Pericet-Camara, R., Viollet, S., Ruffier, F., Brückner, A., Leitel, R., Buss, W., Menouni, M., Expert, F., Juston, R., et al. 2013 Miniature curved artificial

compound eyes. *Proc Natl Acad Sci* **110**, 9267-9272. (doi:10.1073/pnas.1219068110).

[10] Song, Y.M., Xie, Y., Malyarchuk, V., Xiao, J., Jung, I., Choi, K.-J., Liu, Z., Park, H., Lu, C., Kim, R.-H., et al. 2013 Digital cameras with designs inspired by the arthropod eye. *Nature* **497**, 95-99. (doi:10.1038/nature12083).

[11] Fuller, S.B., Karpelson, M., Censi, A., Ma, K.Y. & Wood, R.J. 2014 Controlling free flight of a robotic fly using an onboard vision sensor inspired by insect ocelli. *J R Soc Interface* **11**. (doi:10.1098/rsif.2014.0281).

[12] Duhamel, P.E.J., Perez-Arancibia, N.O., Barrows, G.L. & Wood, R.J. 2013 Biologically Inspired Optical-Flow Sensing for Altitude Control of Flapping-Wing Microrobots. *IEEE-ASME Trans. Mechatron.* **18**, 556-568. (doi:10.1109/tmech.2012.2225635).

[13] Reichardt, W. 1961 Autocorrelation, a Principle for the Evaluation of Sensory Information by the Central Nervous System. In *Sensory Communication* (ed. W.A. Rosenblith), pp. 303-317. New York, Wiley.

[14] Franceschini, N., Riehle, A. & Le Nestour, A. 1989 Directionally selective motion detection by insect neurons. In *Facets of Vision* (eds. D.G. Stavenga & R.C. Hardie), pp. 360-390. Berlin, Germany, Springer.

[15] van de Grind, W.A., Koenderink, J.J. & van Doorn, A.J. 1986 The distribution of human motion detector properties in the monocular visual field. *Vision Res.* **26**, 797-810. (doi:10.1016/0042-6989(86)90095-7).

[16] Maisak, M.S., Haag, J., Ammer, G., Serbe, E., Meier, M., Leonhardt, A., Schilling, T., Bahl, A., Rubin, G.M., Nern, A., et al. 2013 A directional tuning map of Drosophila elementary motion detectors. *Nature* **500**, 212-216. (doi:10.1038/nature12320).

[17] Land, M.F. 1997 Visual Acuity in Insects. *Annu Rev Entomol* **42**, 147-177.

[18] Götz, K.G. 1965 Die optischen Übertragungseigenschaften der Komplexaugen von Drosophila. *Biol Cybern* **2**, 215-221. (doi:10.1007/bf00306417).

[19] Franceschini, N. & Kirschfeld, K. 1971 Les phénomènes de pseudopupille dans l'œil composé deDrosophila. *Kybernetik* **9**, 159-182. (doi:10.1007/bf02215177).

[20] Delbruck, T. & Mead, C.A. 1994 Adaptive photoreceptor with wide dynamic range. In *IEEE International Symposium on Circuits and Systems ISCAS '94* (pp. 339-342 vol.334.

[21] Viollet, S., Godiot, S., Leitel, R., Buss, W., Breugnon, P., Menouni, M., Juston, R., Expert, F., Colonnier, F., #039, et al. 2014 Hardware Architecture and Cutting-Edge Assembly Process of a Tiny Curved Compound Eye. *Sensors* **14**, 21702-21721.

[22] Matić, T. & Laughlin, S.B. 1981 Changes in the intensity-response function of an insect's photoreceptors due to light adaptation. *J. Comp. Physiol.* **145**, 169-177. (doi:10.1007/bf00605031).

[23] Normann, R.A. & Perlman, I. 1979 The effects of background illumination on the photoresponses of red and green cones. *J. Physiol.* **286**, 491-507.

[24] Koenderink, J.J. & Doorn, A.J. 1987 Facts on optic flow. *Biol Cybern* **56**, 247-254. (doi:10.1007/bf00365219).

[25] Expert, F., Viollet, S. & Ruffier, F. 2011 Outdoor field performances of insect-based visual motion sensors. *J. Field Rob.* **28**, 529-541. (doi:10.1002/rob.20398).

[26] Baird, E., Boeddeker, N., Ibbotson, M.R. & Srinivasan, M.V. 2013 A universal strategy for visually guided landing. *Proc Natl Acad Sci* **110**, 18686-18691. (doi:10.1073/pnas.1314311110).

FIGURE 1

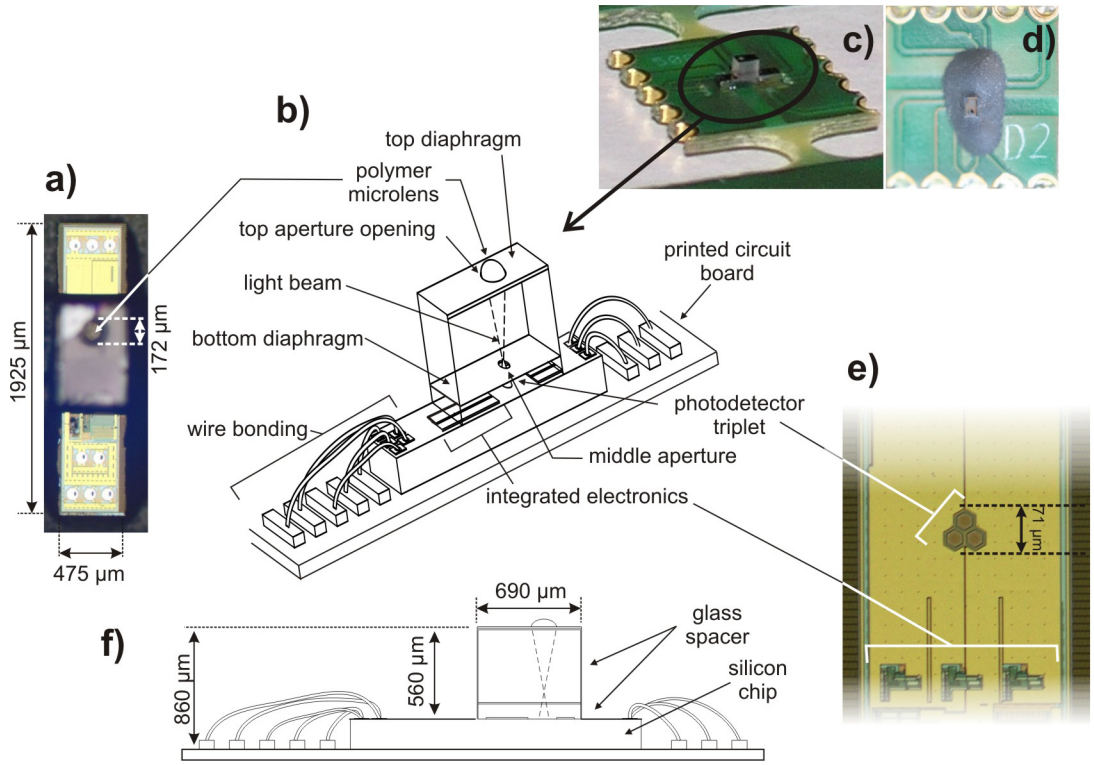

Figure 1. The artificial elementary eye yielding three photodetectors. a) Top-view microscopy image. b) Detailed scheme of the elementary eye and its components. c) Image of the elementary eye mounted on the PCB surface before and d) after glop-top encapsulation. e) Zoomed image of the photodetector triplet without optics. f) Lateral schematic view of the elementary eye.

Figure 2

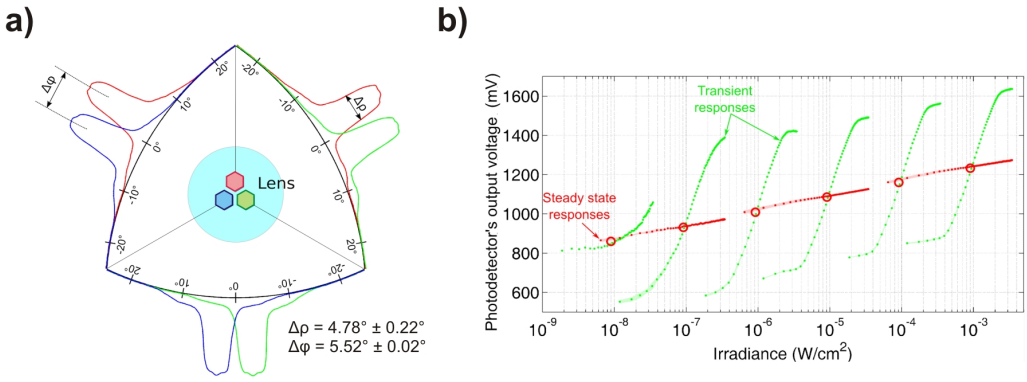

Figure 2. a) Measured angular sensitivity functions (ASF) of the three pairs of photodetectors of the artificial elementary eye. Each colour corresponds to the signal of one of the photodetectors. b) Auto-adaptation of the artificial elementary eye photodetector to ambient light. Measured steady-state (red dots) and transient responses (green dots) of the adaptive analog VLSI photodetectors [20]. Each of the six dynamic operating curves shows the V(log I) response to step increments and decrements of irradiance over about six decades.

FIGURE 3

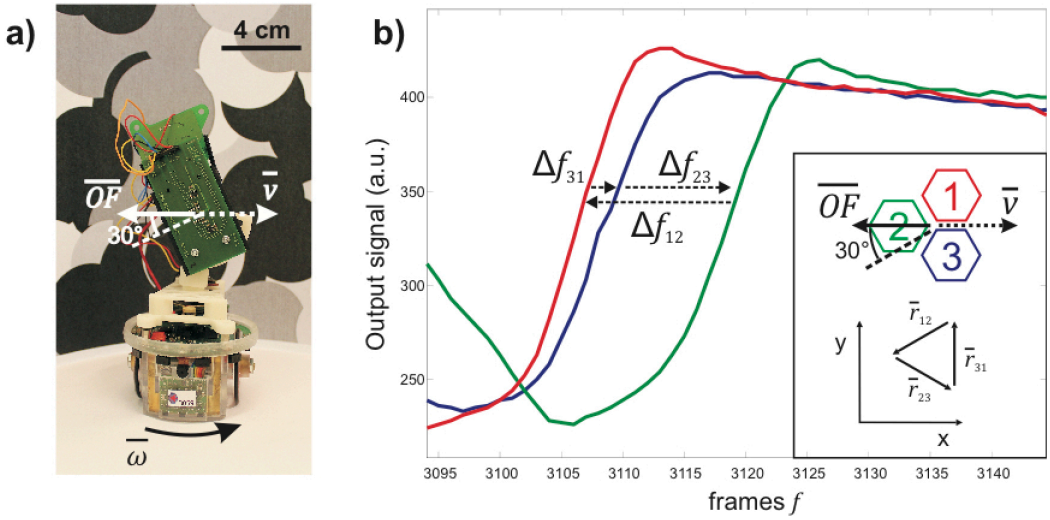

Figure 3. a) Picture of the artificial elementary eye setup mounted on an e-puck robot for an optic flow characterization experiment. The elementary eye is rotated at a roll angle of 30°. b) Graph displaying the output signal of the three photodetectors of the artificial elementary eye versus the frame number during a characterization experiment at 350 fps. Δf_{ij} shows the frame delay between photodetector signals, which is used to calculate the optic flow. The inset displays the orientation of the three photodetectors roll-rotated 30° during the experiment shown in the graph as well as the unit distance vectors r_{ij} for every pair of photodetectors.

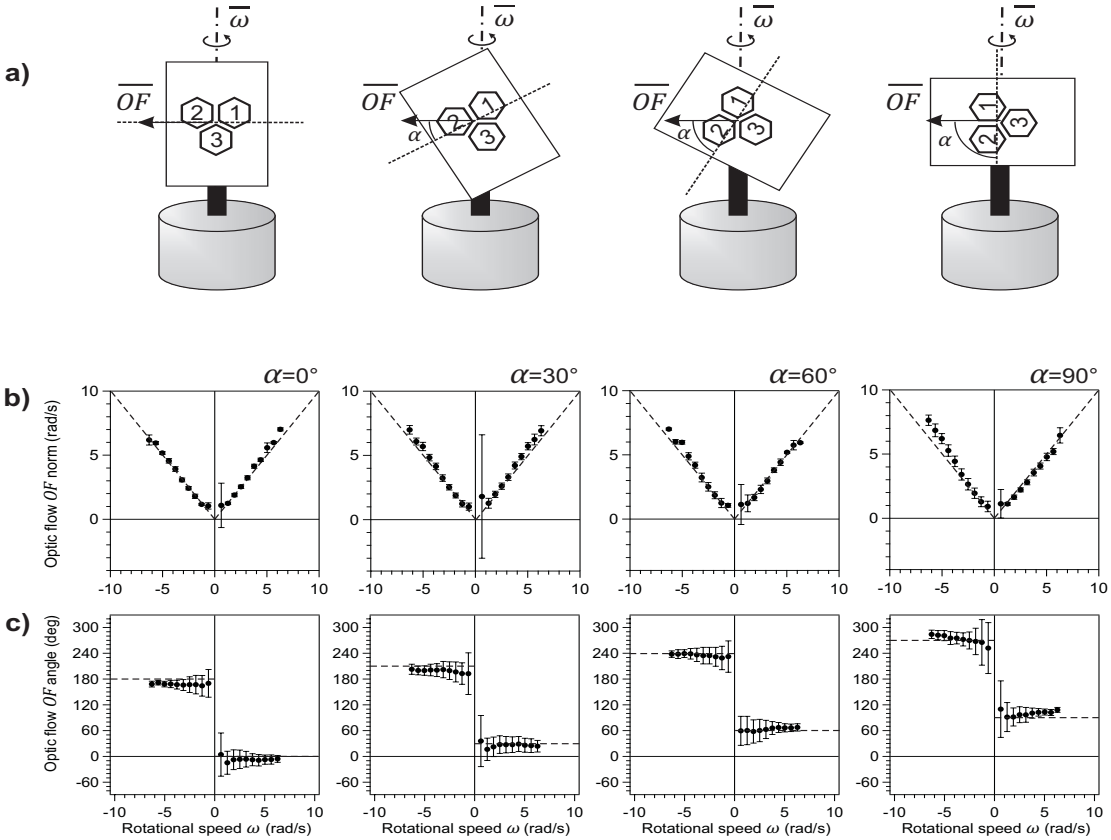

Figure 4. a) Schematic display of the optic flow characterization setup, showing the photodetector triplet and optic flow vector OF measured during yaw rotational motion at angular velocity ω for different α roll angles. b) Optic flow vector norm as a function of yaw rotational speed ω at four α roll angles. Each data point indicates mean and standard deviation of the OF vector norm computed from signals collected during 30 seconds at a frame rate of 350 frames/s. The dashed line shows the theoretical equivalence between OF norm and rotational speed. c) Optic flow vector angle with respect to $\alpha = 0°$ as a function of yaw rotational speed ω at four roll angles α. Each data point indicates mean and standard deviation of OF vector angle values computed from signals collected during 30 seconds at a frame rate of 350 frames/s. The dashed line shows the nominal sensor roll angle α for positive rotational speeds and α +180° for negative ones.

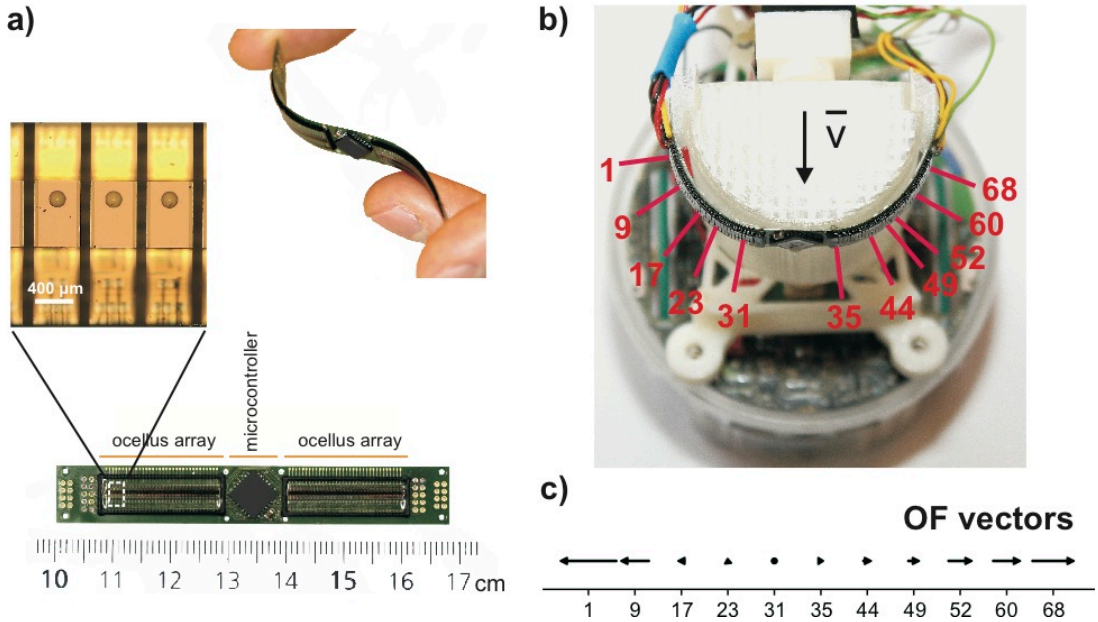

Figure 5. a) A flexible array of 68 artificial elementary eyes and microcontroller for signal extraction. The inset shows a microscopy image of three artificial elementary eyes of the flexible array. b) Top view of the sensor array attached to the characterization setup robot. The red lines indicate the elementary eye whose signals were recorded during the experiment. c) Mean optic flow vectors resulted from a straight and centred trajectory of the robot along a 0.9 meter long and 0.2 meter wide straight corridor (Figure S2) at constant speed of 8 cm/s.

Supplementary Information

Artificial elementary eye parts and assembly

Microoptics. The artificial elementary eyes have been built up from linear arrays of stacks of a microoptics element and an optoelectronics silicon chip, which have been both fabricated on wafers and separated by cutting prior to stacking. The microoptics wafer consists of a microlens array (lenslet diameter of 172 µm) and two diaphragm arrays. The microlenses are formed by reflow of photoresist and subsequent UV-moulding of a highly transparent polymer (Ormocomp, Micro Resist Technology, Berlin, Germany) onto thin display glass (AF32, Schott AG)[9][21]. Low-reflective chromium films are used to create two diaphragm layers, which are deposited by sputtering and patterned by UV photolithography and subsequent metal etching. The optics f-number is 2.4. The resist patterning and the UV-moulding have been carried out utilizing a mask aligner device (Süss Microtec AG, Garching, Germany)

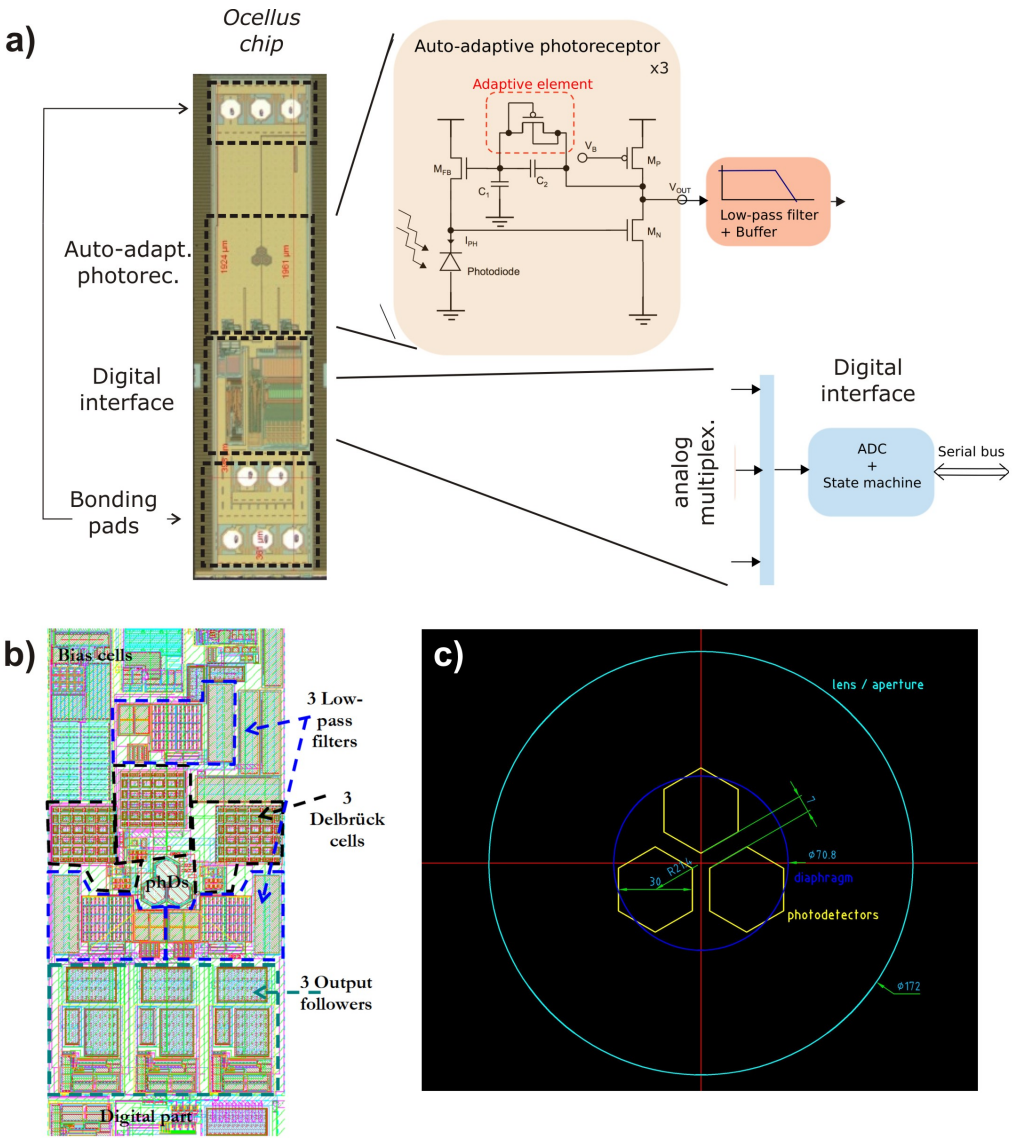

Figure S1. a) Left, top view of the optoelectronic chip of an artificial elementary eye. On the right, basic layout of the photoreceptor processing and read out architecture implemented within each artificial elementary eye. The original circuit proposed by Delbrück and Mead[20] was here enhanced by cascading a first order low-pass filter to prevent temporal aliasing. b) Detailed layout of the electronic circuitry next to the photodetector triplet. c) Dimensions in µm of the components of the photodetector triplet of an artificial elementary eye taken from CAD layout for photo mask fabrication.

Silicon chip. The optoelectronic silicon chip was fabricated in silicon at wafer level using CMOS technology (0.35-µm technology with OPTO option, X-FAB Semiconductor Foundries, Germany). Every chip has a size of 20 x 1.925 mm^2 and consists of 34 columns, each bearing a triplet of hexagonal aVLSI auto-adaptive photodetectors in a triangular arrangement, a bias circuit, a 10-bit analog-to-digital converter (ADC) and a logic circuit that implements a fast serial interface for the read-out protocol (Figure S1a). Every column results in the electronic element of an individual artificial elementary eye after the cutting process (see Assembly process section).

Every auto-adaptive photodetector (Figure S1a) consists of a logarithmic circuit associated with a high-gain negative feedback loop as proposed by Delbrück and Mead[20]. A MOSFET transistor (M_{FB} in Figure S1a) operates in the sub-threshold region where the current-to-voltage characteristic follows a logarithmic law. Thus, the photoreceptor operates over several decades of ambient light level, generating the low gain DC operating curve shown as a red dotted line in Fig. 2b. In addition, transient signals are amplified with a variable gain depending on the equivalent resistance of the adaptive element: the lower the output signal level (V_{out}), the higher the gain. The auto-adaptive feature is used to compensate for ambient light changes, that is, to keep the photodetectors responding to contrasting features even in low or intense ambient lighting. The overall bandwidth of the photoreceptor depends on the current I_{ph} flowing into the photodiode and on the time constants of the amplifier stage. For high ambient lighting levels, the bandwidth can be as large as 500 kHz. To prevent aliasing during the digitization process, we deliberately enhanced the circuit by limiting the bandwidth of each photodetector to about 300 Hz by cascading it with an antialiasing filter, consisting of a first order low-pass filter based on a transconductance amplifier. To limit the dispersion due to the CMOS technology, we finely adjusted the ratio between the two capacitors (C_1 and C_2 in Figure S1a) to minimize the transient gain dispersion of the photodetectors.

Every elementary eye contains a multiplexer and a 10-bit analog-to-digital (ADC) converter of the analog signal of the 3 photodetectors with a conversion time of 15 µs.

Underlying printed circuit board. A rigid square-shaped printed circuit board (PCB) with a surface of 7.6x7.6 mm^2 was fabricated as mechanical and electrical support for the characterization of the artificial elementary eye.

In the case of the bendable elementary eye array, a flexible PCB is used to electrically connect the different artificial elementary eyes with the controlling unit while ensuring their mechanical support. This substrate is a polyimide (KAPTON®) one-layer PCB with a thickness of 100 µm. The low thickness and the absence of vias allow curving the ommatidia down to a radius of curvature of 6.4 mm. In the current approach, the bendability is limited in the centre region due to the rigid microcontroller, which could be placed on a separate board in cases where full flexibility is desired.

On the PCB, tracks for analog and digital power and ground as well as clock, sync, and digital data readout are routed to operate the elementary eye or to all columns of the ocellar array (see Floreano *et al.*[9] and Viollet *et al.*[21] for details on the readout protocol).

Assembly process. The alignment and glue bonding assembly of microoptics, silicon chip, and in the case of the flexible array, on the PCB, is done via a Fineplacer® device that yields a lateral precision down to 1 µm. The glue bonding between the microlens array and optoelectronic silicon chip is realized with a high transparent UV-curing adhesive (OG 146, EPO-TEK Inc., Billerica, United States). In order to improve the bonding strength, a silane-based adhesion promoter has been applied to both surfaces prior to gluing. The glue bonding between the photoreceptor and the PCB is realized applying a thermally curing adhesive (353ND, EPO-TEK).

The silicon chip is electrically connected with the underlying PCB by wedge bonding with aluminium wires of 30 µm. In the case of the ocellar array prototype, the wires are protected with a transparent glob-top material for inspection.

Finally, the rigid optics-electronics stack is cut with a chip saw (DISCO Corp., Japan), a 100-µm thick synthetic-resin-compound dicing blade customized for rigorous and brittle materials, leaving the underlying substrate intact. In the case of individual elementary eyes, every one of the 34 columns is picked after dicing and glued on the square rigid PCBs described before. For the ocellar array, the cutting process is realized with the stack already glued to the flexible PCB, such that the 34 columns are trenched and diced without touching the underlying PCB and its routings. This way, the bendability of the ocellar array is provided.

Characterization methods

Optical sensitivity characterization The optical characterization of the artificial elementary eye implies the characterization of the optical angular sensitivity functions of the three photodetectors. For this, we used the same test bench as the one described in Floreano *et al*[9]. The only difference relies on the use of an additional rotary stage mounted on the axis of the stepper motor in order to select the pair of photodetectors to be characterized. Each pair was selected by rotating 60° the plane of rotation parallel to the triplet plane. Then, the stepper motor was used to rotate the optical axes of each photodetector by steps of 0.1° while recording concomitantly the three photodetector output signals. A 20-Hz flickering point light source based on a white light emitting diode (LED), followed by a diaphragm with a diameter of 1 mm, was placed at a distance of 2.8 m from the photodetectors to illuminate them from a predetermined direction.

Light sensitivity characterization. We developed a programmable lighting box to make the illuminance varying over 7 decades at a distance of 3cm where the artificial elementary eye was placed. The light intensity could be digitally adjusted via digital current driver (ADN8810, Analog Devices) connected to a red LED (TLWR7600, Vishay Semiconductors) through a RS232 bus. This highly controlled light environment allows the response of the elementary eye (photodetector with optics) to be measured both as a function of the steady illuminance and as a function of incremental and decremental light steps presented about the steady illuminance. A direct control of the LED current allowed a variation of the illuminance over 3 decades whereas very low illuminance values were obtained by means of an additional neutral density glass filter (Schott HG3, thickness of 1 or 2mm, optical density OD=2 and Schott HG9, thickness of 2 or 3mm) placed between the LED (Vishay TLWR7600) and the sensor. An additional digital input signal sent by an FPGA was used to synchronize the changes in light intensity with the sensor readout. The irradiance of the light source was measured by means of a radiometer (ILT1700), whose probe was placed at a distance of 28 mm from the light source.

Characterization of optic flow extraction. To characterize the optic flow extraction capabilities, the artificial elementary eye was connected to an external board bearing a microcontroller, and this to an openLog data logger (SparkFun

Electronics Inc., Boulder, CO, USA). The artificial elementary eye communicates with the external board microcontroller via SPI, whereas data are sent to the openLog via UART communication.

The artificial elementary eye uses a direct serial connection with the external microcontroller as readout protocol, similar to the one in the artificial compound eye in Floreano *et al.*[9]. The embedded ADC converts the three-photodetector data at a maximum nominal frequency of 21 kHz. The microcontroller sends frames containing the three values of the photodetector to an SD card via the data logger at a defined frame rate of 350 frames/s.

The whole setup was mounted on an e-puck wheeled robot (http://www.e-puck.org/) using a specially designed mechanical 3D-printed structure (Figure 3a) In this, the sensor is placed at the axis of yaw rotation of the robot, having its viewing direction parallel to the ground. The mechanical support of the elementary eye can be tilted in the perpendicular plane to ground, allowing the rotation of the triplet arrangement and fixation to different roll angles. The robot is placed in the middle of an arena formed by a circular vertical wall patterned with a natural-like image (Figure 3a). The robot is yaw-rotated with various rotational speeds during 30 s. while the visual data are registered in the SD card.

Flexible artificial elementary eye array

Prototype description. The elementary eye array consists of two linear arrays of 34 functional artificial elementary eyes on a flexible substrate, which is a 100μm-thin polyimide printed circuit board. Every elementary eye of the array is wire-bonded to the PCB. Between the two ocellar arrays, a dsPIC33FJ128GP802 microcontroller (Microchip®, Chandler, AZ, USA) carries out readout of the visual data. The readout protocol is a serial direct connection with 7 sync signals, similar to the one used in Floreano *et al.*[9] and Viollet *et al.*[21]. In addition, the microcontroller sends the visual data to an OpenLog data logger through an intermediate board bearing a similar dsPIC microcontroller.

For the validation experiments of the artificial elementary eye array, the prototype is flexed and attached to a 3D-printed semicylindrical piece with 2.4 cm of curvature radius and at a height of 11.3 cm over the ground (Figure S2). During the experiment, the robot is placed in the middle of a 0.2m-wide and 0.9m-long corridor consisting of two parallel walls with a vertically striped black and white pattern. Visual data are collected during its straight trajectory at 8 cm/s until the end of the corridor. The vectors displayed in Figure 5c correspond to the average of the vector modules and angles during a single corridor trajectory measured at individual elementary eyes.

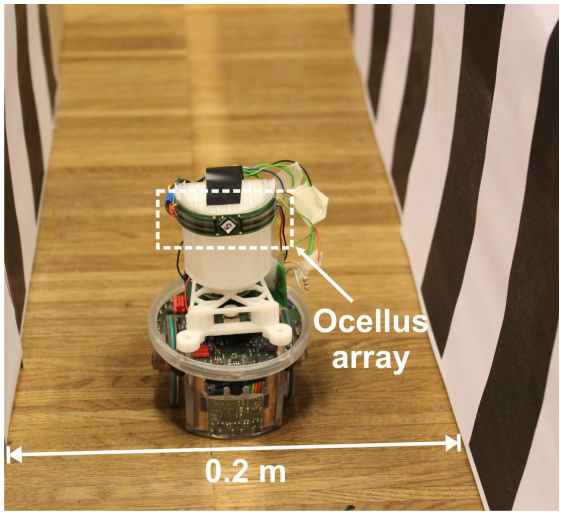

Figure S2. Image of the flexible artificial elementary eye array mounted on a 3D-printed semicylindrical support, and this integrated with an e-puck robot.